This is a preprint of an article published online by Eurpean Journal of Inorganic Chemistry, 2008.

http://www.interscience.wiley.com

Surprising Coordination Geometry Differences in Ce(IV)- and Pu(IV)-Maltol Complexes[1]

Géza Szigethy,[a, b] Jide Xu,[b] Anne E. V. Gorden, [a, b] Simon J. Teat,[c] David K. Shuh,[a] Kenneth N. Raymond[a, b]*

Abstract: As part of a study to characterize the detailed coordination behavior of Pu(IV), single crystal X-ray diffraction structures have been determined for Pu(IV) and Ce(IV) complexes with the naturally-occurring ligand maltol (3-hydroxy-2-methyl-pyran-4-one) and its derivative bromomaltol (5-bromo-3-hydroxy-2-methyl-pyran-4-one). Although Ce(IV) is generally accepted as a structural analog for Pu(IV), and the maltol complexes of these two metals are isostructural, the corresponding bromomaltol complexes are strikingly different with respect to ligand orientation about the metal ion: All complexes exhibit trigonal dodecahedral coordination geometry but the Ce(IV)−bromomaltol complex displays an uncommon ligand arrangement not mirrored in the Pu(IV) complex, although the two metal species are generally accepted to be structural analogs.

Introduction

A detailed understanding of the behavior of actinides and their fission products is fundamental to the development of efficient and well-characterized systems in which these materials are to be used and handled. Examples of such use include solvent extractions for nuclear fuel reprocessing, bio-remediation of contaminated soil at nuclear facilities, and the development of materials suitable for long-term storage of nuclear wastes from the nuclear power industry. While much is known about the solution properties of actinides in specific technologies such as the PUREX process,[2] relatively little is known about the detailed coordination chemistry of transuranics with organic ligands. This, coupled with the significant contribution of plutonium to the amounts of high level materials found in nuclear fuel wastes[3] and the difficulties associated with sequestering Pu(IV) from biological systems[4] has motivated the synthesis and crystallographic characterization of coordination complexes of Pu(IV) bound by a variety of multidentate ligands.

Our development of specific sequestering agents for Pu(IV) has been pursued by exploiting the similarities between Pu(IV) and Fe(III), utilizing ligand types found in siderophores (iron-binding ligands produced by bacteria).[5] One such ligand type found in siderophores are the hydroxypyridinones (HOPOs), which have been part of previous studies of actinide coordination chemistry.[6, 7] A class of structural analogs to HOPOs, and the precursor to substituted 3,4-HOPO, are the hydroxypyrones, one of the simplest of which is 3-hydroxy-2-methyl-pyran-4-one (maltol, $\mathbf{L^1}$, Figure 1). Maltol is most commonly used as a food additive, but is a good transition metal chelator and has been considered for applications as a soluble Fe(III) complex in the treatment of anemia and in iron enriched foods.[8, 9] Some lanthanide complexes with maltol have been synthesized and their formation constants determined.[10] Maltol is an attractive ligand for Pu(IV) coordination chemistry because of its structural similarity to the HOPO ligands, and the crystal structures of Pu(IV)−maltol complexes are of interest for comparison with the Pu(IV)−HOPO structures previously reported.[6] Simple substitutions on the maltol ring provide hydroxypyrones with modified electronic structures to explore the coordination preferences and bonding characteristics of Pu(IV).

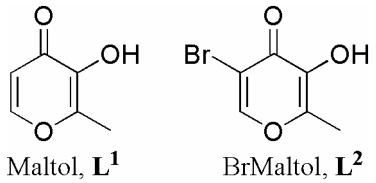

Figure 1. Ligands in this study: 3-hydroxy-2-methyl-pyran-4-one (Maltol, $\mathbf{L^1}$) and 5-bromo-3-hydroxy-2-methyl-pyran-4-one (BrMaltol, $\mathbf{L^2}$).

We report here the synthesis and crystallographic characterization of Pu(IV) complexes with maltol and its derivative bromomaltol (BrMaltol, $\mathbf{L^2}$, Figure 1).[11] Because of their similar charge to ionic radius ratios, Ce(IV) is a generally-accepted structural analog for Pu(IV), and thus the Ce(IV) complexes with $\mathbf{L^1}$ and $\mathbf{L^2}$ have been employed here as structural models for, and

[a] Chemical Sciences Division, Glenn T. Seaborg Center
Lawrence Berkeley National Laboratory
Berkeley, CA, 94720 (USA)
Fax: (510) 486-5283
E-mail: raymond@socrates.berkeley.edu

[b] Department of Chemistry
University of California at Berkeley
Berkeley, CA, 94720-1460 (USA)

[c] Advanced Light Source
Lawrence Berkeley National Laboratory,
Berkeley, CA, 94720 (USA)

Supporting information for this article is available on the WWW under http://www.eurjic.org/ or from the author. It contains shape analysis values, comparison of edge lengths in coordination polyhedra, and ORTEP images of the Ce($\mathbf{L^1}$)$_4$ structure.

species against which to compare, the corresponding Pu(IV) structures. The expectation of structural correlation between the Pu(IV) and Ce(IV) complexes was met in the near identical M($\mathbf{L^1}$)$_4$ crystal structures. However, substitution of $\mathbf{L^2}$ for $\mathbf{L^1}$ led to a dramatic change in the coordination polyhedron about Ce(IV), a result that was surprisingly absent in the analogous Pu(IV) structure.

Results and Discussion

The Ce(IV) complexes with $\mathbf{L^1}$ and $\mathbf{L^2}$ were synthesized in MeOH solutions using Ce(acac)$_4$ (acac = acetylacetonate) as a starting material[12] and crystallized by slow evaporation of CH_2Cl_2 solutions. The corresponding Pu(IV) complexes were synthesized in buffered MeOH/H_2O solutions using a stock solution of Pu(IV) in 1M $HClO_4$ and crystallized by slow evaporation of the mother liquor. All crystal species were highly-colored M$\mathbf{L}_4$ complexes. Crystal parameters are listed in Table 1 and the crystal structures are depicted in Figure 2.

The M($\mathbf{L^1}$)$_4$ complexes are isostructural and crystallize in the tetragonal space group $I4_1/a$ with S_4 crystallographic symmetry and approximate D_{2d} molecular symmetry. As expected from atom charge differences, the M−O(carbonyl) distances are longer than the M−O(phenol) distances, with only slight variation between the Ce−O and Pu−O values (Table 2). Shape analysis[14] reveals the coordination geometry about both metal centers to be closest to that of the trigonal dodecahedron (D_{2d} symmetry). The ligand planes are coincident with the mirror planes in D_{2d} symmetry, and the ligands themselves span the *m* edges of the trigonal dodecahedron according to the notation of Hoard and Silverton (Figure 3).[15]

Like the M($\mathbf{L^1}$)$_4$ complexes, Ce($\mathbf{L^2}$)$_4$ crystallizes in the tetragonal space group $I4_1/a$ with crystallographic $\bar{4}$ symmetry. While shape analysis indicates that the coordination geometry about Ce is again most similar to D_{2d}, the ligands span *g* edges rather than the *m* edges as in the M($\mathbf{L^1}$)$_4$, reducing the molecular symmetry to S_4. The change in geometry is accompanied by a slightly shortened Ce−O(phenol) distance and a significantly lengthened Ce−O(carbonyl) distance.

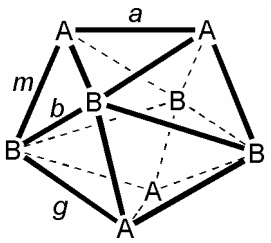

Figure 3. Ideal trigonal dodecahedral polyhedron (D_{2d} symmetry) with edge notation of Hoard and Silverton.[15]

Because there are twice as many *g* edges as *m* edges in a trigonal dodecahedron, there are two ways in which four independent bidentate ligands may span these edges. Interestingly, the geometry observed in the Ce($\mathbf{L^2}$)$_4$ structure is the one not addressed by Kepert as an intermediate between pure D_{2d} and D_{4d} (square antiprismatic) symmetries and seems to be observed here for the first time.[16] Theoretical calculations by Hay *et al.* indicate that this geometry is not an energy minimum for a tetrakis(bidentate) complex.[17] In undistorted trigonal dodecahedra, the *g* edges are longer than the *m* edges, but to accommodate the fixed O(phenol)−O(carbonyl) distance of $\mathbf{L^2}$ along *g* edges the coordination polyhedron distorts along the S_4 axis. Specifically, the *m* edges in Ce($\mathbf{L^2}$)$_4$ are *ca.* 0.36 Å longer than in Ce($\mathbf{L^1}$)$_4$ and the *g* edges a combined 0.36 Å shorter.

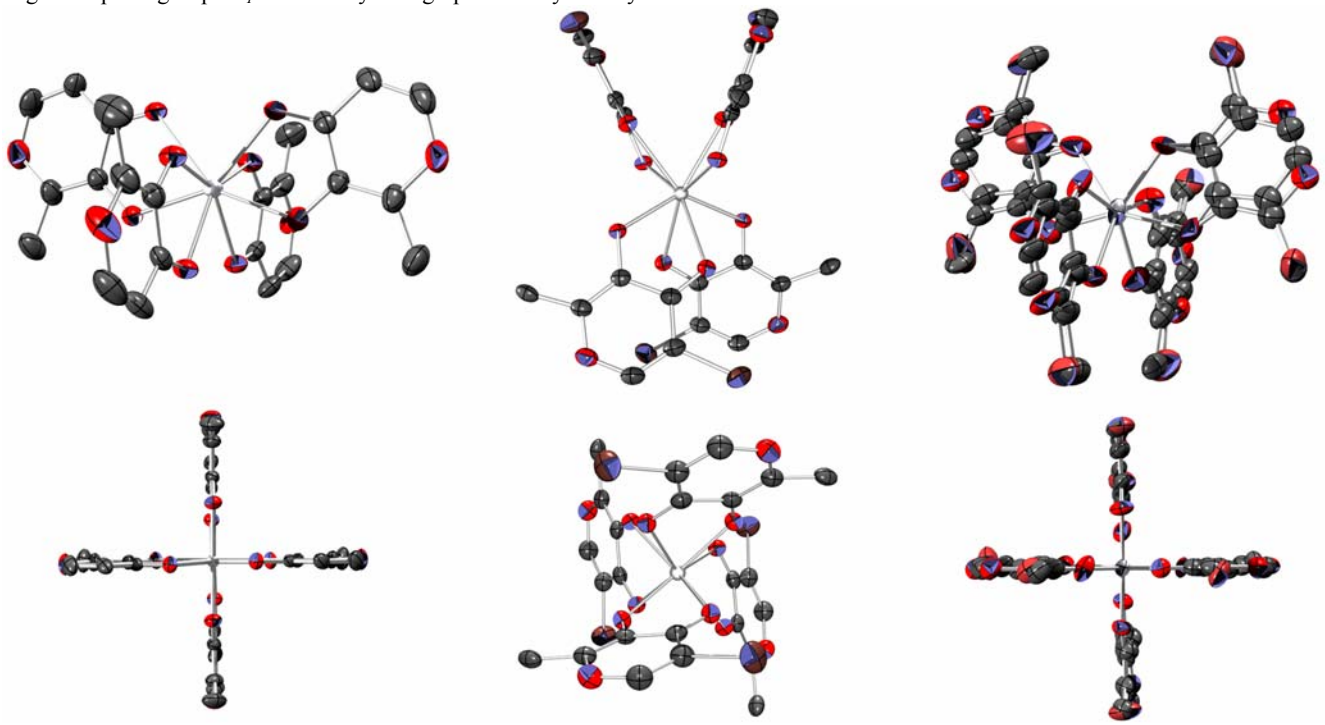

Figure 2. Crystal structures (ORTEP[13]) of Pu($\mathbf{L^1}$)$_4$ (left), Ce($\mathbf{L^2}$)$_4$ (middle), and Pu($\mathbf{L^2}$)$_4$ (right), side and top views. Thermal ellipsoids are drawn at the 50% probability level, hydrogen atoms and solvent inclusions are omitted for clarity. Carbon atoms are depicted as gray, oxygens as red, bromines as brown and metal atoms as silver. The Ce($\mathbf{L^1}$)$_4$ complex is shown in the Supporting Information due to its structural similarity to the Pu($\mathbf{L^1}$)$_4$ structure.

Table 1. Crystal parameters for M($\mathbf{L^n}$)$_4$ complexes

	Ce($\mathbf{L^1}$)$_4$	Ce($\mathbf{L^2}$)$_4$	Pu($\mathbf{L^1}$)$_4$	Pu($\mathbf{L^2}$)$_4$
formula	$CeC_{24}H_{20}O_{12}$	$CeC_{24}H_{16}O_{12}Br_4$	$PuC_{24}H_{20}O_{12}$	$PuC_{24}H_{16}O_{12}Br_4 \cdot 1.7(H_2O)$
M_r	640.52	956.13	742.40	1073.10
T [K]	175(2)	169(2)	193(2)	193(2)
cryst syst	tetragonal	tetragonal	tetragonal	triclinic
space group	$I4_1/a$	$I4_1/a$	$I4_1/a$	$P\ \bar{1}$
color	black	black	red	red
a [Å]	9.2036(4)	14.9502(1)	9.2073(4)	9.1132(19)
b [Å]	9.2036(4)	14.9502(1)	9.2073(4)	9.2739(19)
c [Å]	27.3801(16)	12.9335(2)	27.068(3)	17.458(4)
α [°]	90	90	90	76.180(4)
β [°]	90	90	90	82.495(5)
γ [°]	90	90	90	88.765(4)
V [Å^3]	2319.3(2)	2890.75(5)	2294.7(3)	1420.4(5)
Z	4	4	4	2
ρ_{calcd} [gcm^{-3}]	1.834	2.197	2.149	2.510
μ_{calcd} [mm^{-1}]	2.031	7.152	2.967	8.748
θ range [°]	2.33−26.10	3.43−26.11	2.55−31.15	2.46−24.20
Total reflections	5308	6616	11541	9441
data/restraints/ parameters	1045/0/85	1304/0/94	1442/0/85	4029/685/551
F (000)	1272	1816	1416	997
crystal size [mm^3]	0.09 × 0.08 × 0.06	0.30 × 0.20 × 0.15	0.05 × 0.03 × 0.03	0.02 × 0.01 × 0.01
R1[I > 2σ(I)][a]	0.0320	0.0271	0.0262	0.0890
wR2(all data)[a]	0.0695	0.0669	0.0642	0.2567
GOF[a]	1.212	1.129	1.036	1.085

[a] Definitions: R1 = $\Sigma||F_o| - |F_c||/\Sigma|F_o|$; wR2 = $[\Sigma[w(F_o^2 - F_c^2)^2]/\Sigma[w(F_o^2)^2]]^{1/2}$; GOF = $[\Sigma w(|F_o| - |F_c|)^2/(n-m)]^{1/2}$

Table 2. M-O bond distances and bite angles from the M($\mathbf{L^n}$)$_4$ crystal structures.

	Group 1	Group 2	Group 3	Group 4	Average
Pu−O(phenol) [Å]	2.28(4)	2.25(5)	2.22(4)	2.22(5)	2.24(3)
Pu−O(carbonyl) [Å]	2.34(4)	2.34(5)	2.40(4)	2.37(5)	2.36(3)

[a] Pu−O distances, and bite angle values for Pu($\mathbf{L^2}$)$_4$ are averages of the deconvoluted values in Table 3 (see below).

It was anticipated that the Pu($\mathbf{L^2}$)$_4$ complex would be isostructural with Ce($\mathbf{L^2}$)$_4$ due to the relationship of the M($\mathbf{L^1}$)$_4$ complexes and the similarities in the coordination geometries seen previously in octacoordinate HOPO complexes of Ce(IV) and Pu(IV). The Pu($\mathbf{L^2}$)$_4$ complex does differ in that it crystallizes in the triclinic space group $P\ \bar{1}$ and includes some disordered water of crystallization in the unit cell. Nevertheless, we find the marked difference in coordination geometry surprising. The ligands about the complex exhibit significant disorder between the bromide and methyl substituents resulting from their similar sizes. The structure was modeled using overlapping rigid $\mathbf{L^2}$ rings in both of the possible orientations in a ratio determined by a freely-refining variable. Because of similarities in the degree of disorder observed in each ligand group separately, the extent of ligand disorder was subsequently constrained so that ligand groups opposite each other exhibited the same disorder ratio. Consequently there are two pairs of ligands about the metal modeled with disordered occupancies of 72:28 and 65:35 in which the bromide substituents of ligands opposite each other are oriented in opposite directions (Figure 4).

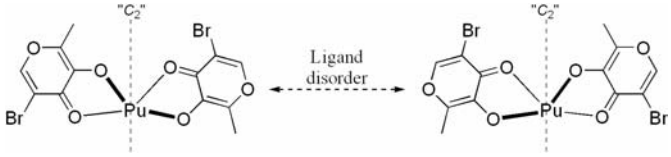

Figure 4. Schematic of the ligand disorder in the Pu($\mathbf{L^2}$)$_4$ crystal structure. The generated "pseudo-C_2" axis is indicated and the shorter Pu−O(phenoxide) bonds in each configuration are indicated in bold. Only one ligand pair is shown here, but the same disorder is seen in the other pair of ligands.

The effect of this coupled disorder is that there is a "pseudo-C_2" axis generated vertically between both pairs of ligands where the S_4 axis would lie in true D_{2d} geometry, with each ligand pair exhibiting this "C_2" axis to a different extent according to the degree of modeled disorder (Figure 4). Because the ligands were modeled as sharing Pu-bound oxygens, shape analysis could be performed and the coordination geometry about Pu is in fact closest to D_{2d}, with the ligands spanning m edges as in the M($\mathbf{L^1}$)$_4$ complexes. A result of the disorder is an averaging of Pu−O bond distances; in $\mathbf{L^2}$ the phenoxide oxygen should bind stronger that the carbonyl oxygen, yet the disorder causes these two bonds to lie on top of each other (Figure 4). The observed bond distances in the Pu($\mathbf{L^2}$)$_4$ structure are thus composites of the two different Pu−O distances according to Equations 1 and 2 in which Pu−O1 and Pu−O2 are the short and long Pu−O distances observed for each ligand group, z is the free variable describing the extent of disorder, and x and y are the calculated Pu−O(phenoxide) and Pu−O(carbonyl) distances respectively. The values of x and y determined by this treatment are shown in Table 3.

$$\text{Pu-O1} = (z)x + (1-z)y \qquad (1)$$

$$\text{Pu-O2} = (1-z)x + (z)y \qquad (2)$$

Table 3. Calculated Pu−O distances in the Pu($\mathbf{L^2}$)$_4$ crystal structure from each disordered ligand group.

Complex	M-O(phenol) [Å]	M-O(carbonyl) [Å]	Bite angle [°]
Ce($\mathbf{L^1}$)$_4$	2.276(3)	2.441(3)	67.55(10)
Ce($\mathbf{L^2}$)$_4$	2.245(3)	2.503(3)	67.47(9)
Pu($\mathbf{L^1}$)$_4$	2.286(3)	2.419(3)	67.93(10)
Pu($\mathbf{L^2}$)$_4$[a]	2.24(3)	2.36(3)	66.98(68)

The deconvoluted Pu−O bond lengths do not differ from each other as much as the Ce−O bonds in Ce($\mathbf{L^2}$)$_4$, but on average the Pu−O(phenoxide) distance is shorter than the Pu−O(carbonyl) distance, a result that supports the validity of the model used in the crystal structure of Pu($\mathbf{L^2}$)$_4$. In both the major and minor disordered geometries there is a C_2 axis of symmetry bisecting one pair of b edges of the coordination polyhedron. Figure 5 illustrates this symmetry schematically in comparison to that in Ce($\mathbf{L^2}$)$_4$. The edges drawn in bold represent those spanned by the ligand, and the arrow heads point in the direction of the bromine substituents. Thus, from the D_{2d} geometry present in the M($\mathbf{L^1}$)$_4$ complexes, the symmetry of Pu($\mathbf{L^2}$)$_4$ has dropped to C_2 with the loss of the S_4/C_2 axis and the removal of mirror planes of symmetry.

Conclusions

Because Pu($\mathbf{L^2}$)$_4$ crystallizes with disordered water molecules in the lattice while the other crystals have no solvent of crystallization, one might argue that the dramatic difference

between the Pu($\mathbf{L}^2$)$_4$ and Ce($\mathbf{L}^2$)$_4$ structures is due to crystal packing effects. To us this seems unlikely; We speculate that the larger role of both *f* and *d* orbital bonding in Pu(IV) compared to Ce(IV)[18] explains this difference and further studies are underway to explore this conjecture.

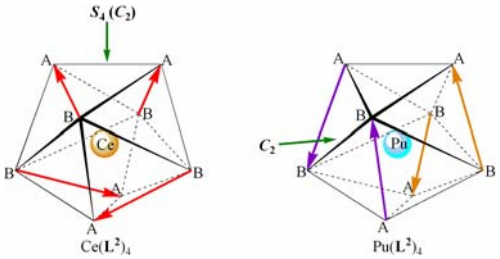

Figure 5. Coordination polyhedra of the M($\mathbf{L}^2$)$_4$ complexes with spanned edges indicated by arrows whose heads point towards the bromide substituent. Arrows related by symmetry have the same color, with molecular symmetry axes indicated.

Experimental Section

General methods: Purification and synthetic procedures with ^{242}Pu were conducted in a glove box under negative pressure designed for the safe handling of radionuclides. Liquid scintillation counting was performed with a Wallac Guardian 1414 liquid scintillation counter, and the scintillation cocktail was Eco-Lume (ICN). Bulk electrolysis using a Ag/AgCl reference electrode was conducted in a scintillation vial fitted with a stir bar, a platinum mesh working electrode, an Ag/AgCl reference electrode, and a platinum counter electrode. An IBM Voltammic analyzer was used to adjust the potential. 2-Maltol was purchased from Aldrich and used as received. Water was distilled and further purified by a Millipore cartridge system (resistivity 18×10^6 Ω). NMR spectra were collected using a Bruker AMX-400 spectrometer in $CDCl_3$. Organic starting materials were purchased from commercial sources and used without purification or were synthesized following literature procedures.

Pu(IV) stock solution preparation: ^{242}Pu was received from Oak Ridge National Laboratory as PuO_2 (lot Pu-242-327 A, 99.93 wt. % of metal ^{242}Pu). The solid was dissolved in concentrated nitric acid with heating. The ^{242}Pu stock solution was loaded onto a nitrate-activated 400 mesh Dowex anion exchange resin column and washed with several column volumes of 7.5 M HNO_3 to remove any daughter products; the ^{242}Pu was isolated as the nitrate. The plutonium was then eluted with 0.4 M HCl with a trace of HF to strip the Pu(IV) from the column. The plutonium eluent was then transferred to a round-bottomed boiling flask fitted with a condensing arm and KOH traps to collect acid vapors, and boiled to dryness. The remaining salt was dissolved in concentrated HNO_3 and boiled for three hours to digest any organic material present in the sample. The solution was concentrated by evaporation. Concentrated perchloric acid was added to the solution, and it was boiled for three hours. Fresh perchloric acid was continually added to maintain the solution volume until the nitrate was removed. The resulting characteristically yellow Pu(VI) solution in concentrated perchloric acid was diluted with water to reach a final concentration of approximately 1M perchloric acid. This solution was adjusted to Pu(III) by electrochemical reduction and then oxidized to Pu(IV) before use in reactions. An aliquot of this solution was diluted with deionized water to 1.0 M $HClO_4$ and the Pu concentration was determined by alpha liquid scintillation to be 0.006 M.

Ce($C_6H_5O_3$)$_4$ [Ce($\mathbf{L}^1$)$_4$]: A solution of Ce(acac)$_4$ (50 mg, 0.093 mmol) in MeOH (2.5 mL) was added to a stirred solution of $\mathbf{L}^1$ (48 mg, 0.38 mmol) in MeOH (2.5 mL). Stirring was stopped and the solution was allowed to stand in the freezer for 2 days, precipitating out a dark microcrystalline solid which was filtered and washed with cold MeOH. The solid was dried under vacuum yielding 52 mg of a purple/black powder (87%). ^{1}H NMR ($CDCl_3$): δ = 2.37 (s, 12H, CH_3), δ = 6.45 (d, $J_{(H,H)}$ = 4.8 Hz, 4H, CH), δ = 7.69 (d, $J_{(H,H)}$ = 4.8 Hz, 4H, CH) ppm. X-ray quality crystals were grown by slow evaporation of a CH_2Cl_2 solution.

Ce($C_6H_4O_3Br$)$_4$ [Ce($\mathbf{L}^2$)$_4$]: Ce(acac)$_4$ (100 mg, 0.19 mmol) and $\mathbf{L}^2$ (153 mg, 0.75 mmol) were dissolved in MeOH (5 mL) at room temperature. A purple/black microcrystalline solid quickly formed, and after stirring for three hours and cooling in a freezer the solid product was filtered and washed with cold MeOH. The solid was dried under vacuum yielding 157 mg of a purple/black powder (88%). ^{1}H NMR ($CDCl_3$): δ = 2.37 (s, 12H, CH_3), δ = 3.49 (s, 3H, CH_3OH), δ = 8.01 (s, 4H, CH) ppm. X-ray quality crystals were grown by slow evaporation of a CH_2Cl_2 solution.

Pu($C_6H_5O_3$)$_4$ [Pu($\mathbf{L}^1$)$_4$]: To a solution of $\mathbf{L}^1$ (0.9 mg, 7.1 μmol) in 2 M NH_4OAc (150 μL) and MeOH (250 μL) was added 6 mM Pu(IV) in ca. 1 M $HClO_4$ (298 μL, 1.8 μmol) (M:L = 1:3.9). The solution turned orange and was allowed to evaporate slowly over three days, depositing red crystals from which X-ray quality crystals were removed for structural analysis.

Pu($C_6H_4O_3Br$)$_4$ [Pu($\mathbf{L}^2$)$_4$]: To a solution of $\mathbf{L}^2$ (1.6 mg, 7.8 μmol) in 2 M NH_4OAc (230 μL) and MeOH (500 μL) was added 6 mM Pu(IV) in ca. 1 M $HClO_4$ (327 μL, 1.9 μmol) (M:L = 1:4.1). The solution turned orange and was allowed to evaporate slowly over three days, depositing red crystal clusters from which X-ray quality crystals were cut for structural analysis.

X-ray Diffraction Data Collection: Ce(IV) crystals were mounted on glass fibers with oil and X-ray diffraction data was collected using a Bruker SMART 1000 detector with Mo-K_α radiation (λ = 0.71073 Å) at the UC Berkeley X-ray crystallographic facility. Pu(IV) crystals were mounted in oil inside a quartz capillary which was sealed by epoxy and coated with nail polish to prevent shattering. Data for the Pu complexes were collected using a Bruker APEX II detector with synchrotron radiation ($h\upsilon$ = 16 keV, λ = 0.7749 Å) at Beamline 11.3.1 at the Advanced Light Source at LBNL. All data was collected using ω-scans and were integrated by the program SAINT.[19, 20] The data were corrected for Lorentz and polarization effects. Data were analyzed for agreement and possible absorption using XPREP and a multi-scan absorption correction was applied in SADABS.[21, 22] Equivalent reflections were merged without an applied decay correction. Both Ce structures and the Pu($\mathbf{L}^1$)$_4$ structure were solved by direct methods, while the Pu($\mathbf{L}^2$)$_4$ structure was solved by Patterson methods,[23, 24] and all structures were expanded using Fourier techniques using the SHELXL package.[23] Least squares refinement of F against all reflections was carried out to convergence with R[I > 2σ(I)]. All non-hydrogen atoms were refined anisotropically with the exception of solvent atoms. Hydrogen atoms were fixed in geometric positions, and torsion angles about methyl groups were refined using the riding model where possible. Further refinement details are reported in the .cif files in the Supporting Information.

CCDC-672167-672170 contain the supplementary crystallographic data for this paper. These data can be obtained free of charge from The Cambridge Crystallographic Data Centre via www.ccdc.cam.ac.uk/data_request/cif.

Supporting Information (see footnote on the first page of this article): Contains shape analysis values, comparison of edge lengths in coordination polyhedra, and ORTEP images of the Ce($\mathbf{L}^1$)$_4$ structure.

Acknowledgments

We thank Dr. Allen Oliver for help with data collection and Dr. Fred Hollander at the UC Berkeley X-ray facility for help in structure modeling. This research and the ALS are supported by the Director, Office of Science, Office of Basic Energy Sciences (OBES), and the OBES Division of Chemical Sciences, Geosciences, and Biosciences of the U.S. Department of Energy at LBNL under Contract No. DE-AC02-05CH11231.

[1] This paper is #59 in the series "Specific Sequestering Agents for the Actinides." For the previous paper, see reference number 7.
[2] A. P. Paiva, P. Malik, *J. Rad. Nuc. Chem.* **2004**, *261*(2), 485-496.
[3] Nuclear Development; Advanced Nuclear Fuel Cycles and Radioactive Waste Management. *Nuclear Energy* **2006**, (4), 1-248.
[4] A. E. V. Gorden, J. Xu, K. N. Raymond, *Chem. Rev.* **2003**, *103*, 4207-4282.
[5] F. L. Weitl, K. N. Raymond, W. L. Smith, T. R. Howard, *J. Am. Chem. Soc.* **1978**, *100*(4), 1170-1172.
[6] a) A. E. V. Gorden, D. K. Shuh, B. E. F. Tiedemann, R. E. Wilson, J. Xu, K. N. Raymond, *Chem. Eur. J.* **2005**, *11*, 2842-2848. b) A. E. V. Gorden, D. K. Shuh, B. E. F. Tiedemann, R. E. Wilson, J. Xu, K. N. Raymond, *Chem. Eur. J.* **2007**, *13*, 378.
[7] A. E. V. Gorden; J. Xu, G. Szigethy, A. Oliver, D. K. Shuh, K. N. Raymond, *J. Am. Chem. Soc.* **2007**, *129*(21), 6674-6675.
[8] M. T. Ahmet, C. S. Frampton, J. Silver, *J. Chem. Soc., Dalton Trans.* **1988**, 1159-1163.
[9] K. H. Thompson, C. A. Barta, C. Orvig, *Chem. Soc. Rev.* **2006**, *35*, 545-56.
[10] K. Dutt, U. V. M. Sharma, *J. Inorg. Nucl. Chem.* **1970**, *32*, 1035-1038.
[11] J. H. Looker, R. J. Prokop, W. E. Serbousek, M. D. Cliffton, *J. Org. Chem.* **1979**, *44*(19), 3408-10.
[12] T. J. Pinnavaia, R. C. Fay, *Inorg. Synth.* **1970**, *12*, 77-80.
[13] Ortep-3 for Windows: L. J. Farrugia, J. Appl. Cryst , **1997**, *30*, 565.
[14] J. Xu, E. Radkov, M. Ziegler, K. N. Raymond, *Inorg. Chem.* **2000**, *39*, 4156-4164.
[15] J. L. Hoard, J. V. Silverton, *Inorg. Chem.* **1963**, *2*(2), 235-242.

[16] D. L. Kepert, *Inorganic Stereochemistry*. Springer-Verlag: New York, **1982**.
[17] B. P. Hay, J.Uddin, T. K. Firman, *Polyhedron* **2004**, *23*, 145-54.
[18] A. J. Gaunt, S. D. Reilly, A. E. Enriquez, B. L. Scott, J. A. Ibers, P. Sekar, K. I. M. Ingram, N. Kaltsoyannis, M. P. Neu, *Inorg. Chem.* **2008**, *47*(1), 29-41.
[19] SAINT: SAX Area-Detector Integration Program, V.6.40; Bruker Analytical X-ray Systems, Inc.: Madison, WI, **2003**.
[20] SAINT: SAX Area-Detector Integration Program, V.4.024; Siemens Industrial Automation, Inc, Madison, WI, **1995**.
[21] XPREP (V.6.12), Part of SHELXTL Crystal Structure Determination Package; Bruker Analytical X-ray Systems, Inc.: Madison, WI, **2001**.
[22] SADABS: Bruker Nonius Area Detector Scaling and Absorption V. 2.05; Bruker Analytical X-ray Systems, Inc.: Madison, WI, **2003**.
[23] SHELXTL (V.5.10), SHELXTL Crystal Structure Determination Package; Bruker Analytical X-ray Systems, Inc.: Madison, WI, **1997**.
[24] SIR92: A. Altomare, M. C. Burla, M. Camalli, M. Cacarano, C. Giacavazzo, A. Guagliardi, G. Polidori, *J. Appl. Cryst*. **1994**.